EPR and SQUID interrogations of Cr(III) trimer complexes in the MIL-101(Cr) and bimetallic MIL-100(Al/Cr) MOFs

Kavipriya Thangavel[1,2], Andrea Folli[2], Michael Ziese[1], Steffen Hausdorf[3], Stefan Kaskel[3], Damien M. Murphy[2], and Andreas Pöppl[1*]

1 Felix Bloch Institute for Solid State Physics, University of Leipzig, Linnestrasse. 5, 04103 Leipzig, Germany
2 School of Chemistry, Cardiff University, Park Place, Cardiff CF10 3AT, UK
3 Department of Inorganic Chemistry, Technische Universität Dresden, Bergstrasse 66,01069 Dresden, Germany
* poeppl@physik.uni-leipzig.de

August 1, 2022

Abstract

Herein, electron paramagnetic resonance (EPR) spectroscopy at X- (9.4 GHz), Q- (34 GHz) and W-band (95 GHz), and superconducting quantum interference device (SQUID) measurements on antiferromagnetically coupled metal trimers in MIL-101(Cr) and MIL-100(Al$_{0.8}$Cr$_{0.2}$) MOFs were investigated. At low temperatures, the Cr(III) trimers exhibit a Dzyaloshinsky-Moriya (D-M) interaction, and have a total spin state $S_T = 1/2$.

1 Introduction

Metal-organic frameworks (MOFs) are a novel and the most prominent class of microporous materials for the applications such as gas storage and separation, catalysis, heat storage, sensing, electrochemical energy, supercapacitors and liquid purification, owing to their unique structural diversity and tunability [1–5]. The structured and tunable pore nature, enormous surface and volume area, crystal integrity and low density are just some of the salient properties of MOFs, which make MOFs a revolutionary materials for numerous applications including device fabrication, chemical and technological industries [3–5]. In recent years, the magnetic behaviors of MOFs are getting attention in the field of molecular magnetism since they consist of a paramagnetic secondary building unit (SBU) along with the organic connecting linker [6]. Among MOFs, MIL (Materials Institute Lavoisier) -101 and MIL-100 MOF families are complex MOFs in crystal structure just with a single linker and SBU. In addition, these MOFs have pores in two different sizes [7] (29 Å and 34 Å for MIL-101; 25 Å and 29 Å for MIL-100) that allow the adsorption of gas and liquid [8,9]. MIL-101(M) and MIL-100(M) frameworks contain trinuclear metal ions $M(III)_3$ in the octahedral units, and four trimers, forming a supertetrahedron. In MIL-100, the trimers are connected through benzene tricarboxylate (BTC) linker and in MIL-101, the linker is benzene dicarboxylate (BDC) [8]. Understanding the pairwise magnetic exchange interaction in the metal trimer clusters is complicated, and the term magnetic 'frustration' (Figure 4b in Appendix A) often describes this situation [10]. The influence of antisymmetric exchange on the electronic properties of trinuclear $Cu(II)_3$ metal complexes was experimentally observed for the first time by Tsukerlat *et al* [10,11]. Likewise, antisymmetric exchange interaction of $Cr(III)_3$ trimer cluster was experimentally investigated by M. Honda *et al.*, [12] A. Vlachos *et al.*, [13] A. Figuerola *et al.*, [14] by means of superconducting quantum interference device (SQUID) and electron paramagnetic resonance (EPR) spectroscopy. Furthermore, the role played by the guest-framework intermolecular interactions, influence of adsorption on the intramolecular interactions and the changes in the internal structure can be elucidated by tracking the paramagnetic species in the SBU [6,9,15–18]. In this regard, EPR spectroscopy is one of the inevitable tools to understand the change in the local structure of MOFs due to guest molecular interaction during *ex situ* [16] and *in situ* [15,17] gas adsorption, liquid adsorption, post synthetically modified ion exchange, [2] and inter molecular magnetic couplings [2,19,20] by monitoring the behavior of paramagnetic metal ions in the SBU.

   Herein, we studied and discussed the local structure and the intramolecular interaction of EPR active Cr(III) trimer complex of the MIL-101(Cr) and magnetically diluted bimetallic MIL-100($Al_{0.8}Cr_{0.2}$) MOFs with $Al(III)_{3-x}Cr(III)_x$ units for the comparison by means of SQUID magnetometer and multi-frequency EPR spectroscopy techniques.

2 Experimental Details

Metal-organic frameworks MIL-101(Cr) and MIL-100($Al_{0.8}Cr_{0.2}$) were purchased from commercial MOF seller 'Materials Center, Technische Universität Dresden'. In MIL-100(Al/Cr), 20% Cr has been incorporated on Al sites within the frameworks. All the experiments mentioned below were done on the as-synthesized MIL-101(Cr) and MIL-100($Al_{0.8}Cr_{0.2}$) MOFs.

   The magnetization measurements were performed using a SQUID magnetometer (Quantum Design MPMS XL). Hysteresis loops at several temperatures between ± 7 T as well as the temperature-dependence at 0.5 T in the temperature range of 4 K to 300 K were measured.

   Continuous wave (cw) X-band (∼ 9.5 GHz) EPR spectra were measured at temperature ranging from $T = 7$ K to $T = 290$ K by means of a Bruker EMXmicro spectrometer fitted with a Bruker ER4119HS cylindrical cavity using an He cryostat ESR900, Oxford instruments. In all

X-band experiments, the microwave (mW) power was set to 2 mW, modulation frequency was kept as 100 kHz, and modulation amplitude was maintained to 10 G to acquire a spectrum without any line shape distortion and saturation. Cw Q-band ($\sim$34 GHz) EPR spectra were performed using Bruker EMX 10-40 spectrometer fitted with cylindrical cavity and an Oxford Instruments CF935 cryostat at $T = 20$ K and 295 K. In Q-band, the experimental parameters, the mW power, modulation frequency and modulation amplitude were set to 1.8 mW, 100 kHz and 20 G, respectively. Unlike X- and Q-band EPR spectrometers, the high magnetic field of W- band ($\sim$95 GHz) EPR requires a superconducting magnet (Bruker 6T SC) and measured using an Elexsys E600 spectrometer equipped with a Bruker E600-1021H TeraFlex resonator, and the spectra were recorded at $T = 20$ K and 300 K. For W-band experiments, the microwave power kept as either 5 μW or 50 μW depending on the signal quality. The EPR intensities of the X-band signals ranging from $T = 7$ K to $T = 280$ K (Figure 2) were extracted by taking double integration of the full EPR spectrum.

The exchange Hamiltonian for the Cr(III) trimers can be written as [12, 21],

$$\mathscr{H}_{Ex} = -2J_0(\hat{S}_1.\hat{S}_2 + \hat{S}_2.\hat{S}_3 + \hat{S}_3.\hat{S}_1) - 2J_1(\hat{S}_3.\hat{S}_1), \tag{1}$$

where $\hat{S}_1$, $\hat{S}_2$ and $\hat{S}_3$ are the Cr(III) spin operators with single $S_i = 3/2$ spins for each chromium ion. J_0 is the main exchange parameter and $|J_1/J_0| \ll 1$. Eqn.1 results in five degenerate energy levels corresponding to the total spin states $S_T = 1/2, 3/2, 5/2, 7/2$ and $9/2$ of the trimer with the twofold degenerate $S_T = 1/2$ state being the ground state in case of antiferromagnetically (AFM) coupled trimers. The degeneracy of the $S_T = 1/2$ state is lifted for $J_1 \neq 0$ [12].

Also, the Hamiltonian of inter-trimer interaction can be defined by [12, 21],

$$\hat{\mathscr{H}}_{in} = -2J_{in}(S_{iT}.S_{jT}), \tag{2}$$

where S_{iT} and S_{jT} correspond to the total spins of i-th and j-th trimers, respectively. In case of EPR experiments, the additional terms

$$\mathscr{H} = \mu_B B\mathbf{g}(\hat{S}_1 + \hat{S}_2 + \hat{S}_3) + \sum_{i=1}^{3}(D_{ZFS,i}\{S_{i,z'}^2 - S_i[S_i + 1]/3\} + E_{ZFS,i}\{S_{i,x'}^2 - S_{i,y'}^2\}) +$$
$$D(\hat{S}_1 \times \hat{S}_2 + \hat{S}_1 \times \hat{S}_3 + \hat{S}_2 \times \hat{S}_3) \tag{3}$$

must be considered in the spin-Hamiltonian for the Cr(III) trimers, where the first term represents the Zeeman interaction between $S = 3/2$ electron spins of the chromium ions and the external magnetic field (μ_B is the Bohr magneton, $\mathbf{g}$ is the g-tensor, B is the external magnetic field). The second term corresponds to the zero field splitting (ZFS) with the axial and rhombic ZFS parameters $D_{ZFS,i}$ and $E_{ZFS,i}$ and the third term describes the antisymmetric exchange contribution caused by the Dzyaloshinsky-Moriya (D-M) interaction. Here D is a pseudo-vector directed perpendicular to a plane defined by the Cr(III) ions in the trimers [12].

3 Results and Discussion

3.1 SQUID magnetometry results

Figure 1 shows the temperature variation of zero-field-cooling (ZFC), field cooled cooling (FCC) and field cooled warming (FCW) magnetic susceptibility behavior of MIL-101(Cr) and MIL-100(Al$_{0.8}$Cr$_{0.2}$) MOFs obtained in 0.5 T magnetic field. The M-T (magnetization vs temperature) behavior of both the MOFs suggests a paramagnetic nature. The paramagnetic susceptibility of both the MOFs follows Curie-Weiss (C-W) law (eqn. 4) for temperatures $T > 15$ K

(MIL-101(Cr) and $T > 120$ K (MIL-100(Al$_{0.8}$Cr$_{0.2}$)). The fitted parameters (Figure 1a & 1b insets) yield effective paramagnetic moment (μ_{eff}) and paramagnetic Curie temperature (θ_p) values as -82 K and 5.43 μ_B/f.u. (f.u.-formula unit), respectively for MIL-101(Cr) MOF. While for MIL-100(Al$_{0.8}$Cr$_{0.2}$), it is -87 K and 3.14 μ_B/f.u., respectively. The occurrence of a negative sign of θ_p of both the MOFs indicates the existence of AFM interactions in the system.
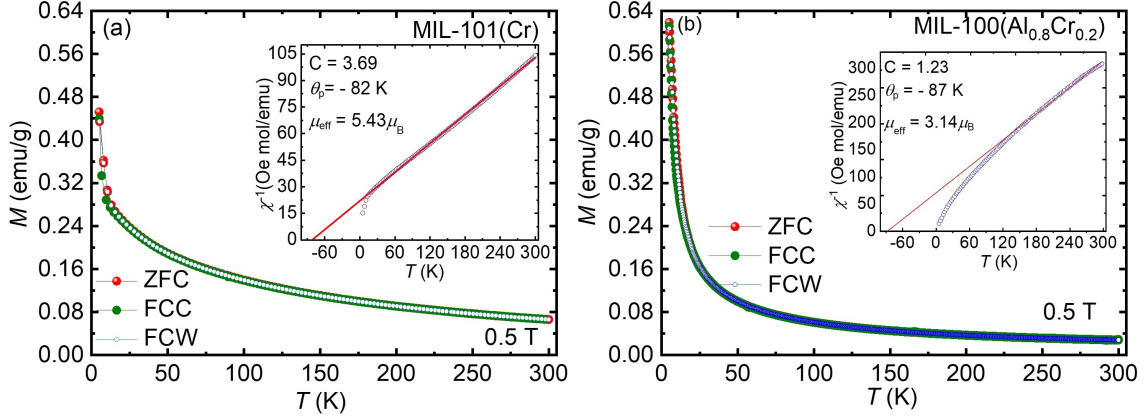
Figure 1: ZFC, FCC and FCW M-T curves of (a) MIL-101(Cr), and (b) MIL-100(Al$_{0.8}$Cr$_{0.2}$) with an applied field of 0.5 T. (Insets: The temperature-dependence of the reciprocal of the magnetic susceptibility of its corresponding ZFC curves.)

The magnetic susceptibility can be written as

$$\chi = \frac{C}{T - \theta_p} \tag{4}$$

where, χ is the magnetic susceptibility, C is the Curie constant, and θ_p is the paramagnetic Curie temperature.

Also, μ_{eff} was calculated using the following relation,

$$\mu_{eff} = \sqrt{\frac{3k_B C}{N \mu_B^2}} = \sqrt{8C} \tag{5}$$

where, μ_{eff} is the effective Bohr magneton, k_B is the Boltzmann constant, C is the Curie constant, N is the Avogadro number and μ_B is the electron Bohr magneton. ZFC, FCC, and FCW curves for both materials are identical (Figure 1), and No magnetic hysteresis effects at any temperatures were observed, as shown by field-dependent magnetization measurements (Figure 5 in Appendix B).

For MIL-101(Cr) the overall temperature-dependence of χ^{-1} is typical for Cr(III) trimers [12, 13, 16]. Therefore, using [12, 13, 16]

$$\theta_p = 5 \frac{(J_0 + \frac{J_1}{3})}{k_B} \tag{6}$$

we can estimate $J_0 = $ -11.4 cm^{-1} for MIL-101(Cr) from the susceptibility data at T > 15 K. Here, we assumed $J_0 \gg J_1$ as we could not determine J_1 from the magnetization measurements. According to Honda *et al.* [12] the steep drop in χ^{-1} at low temperatures T < 15 K can be associated with the inter-trimer interaction and provides a lower limit for a second Curie temperature-like parameter $\theta'_p > $ -6 K (Figure 6 in Appendix B) where

$$\theta'_p = \frac{n J_{in}}{4 k_B} \tag{7}$$

In the case of MIL-101(Cr) with its supertetrahedral structure of the connected Cr(III) trimers [8] n = 3 provides $|J_0| > |J_{in}|$ (J_{in} = -5.6 cm^{-1}).

In the case of MIL- 100(Al$_{0.8}$Cr$_{0.2}$), the χ^{-1} temperature-dependence does not give an indication of the presence of Cr(III) trimers but displays a rather unspecific response of one or several AFM coupled spin systems. Assuming again a further contribution dominating the magnetization data at T < 30 K and applying eqn. 4, we can roughly estimate the lower limit for a second Curie temperature like parameter $\theta_p^{'}$ > -1.8 K (Figure 6 in Appendix B). The small limit $|\theta_p^{'}|$ might indicate a very weak inter-trimer exchange between various Al(III)$_{3-x}$Cr(III)$_x$ units or just a simple paramagnetic contribution due to isolated Cr(III) ions.

3.2 EPR spectroscopy results

For comparison with magnetization data, the temperature-dependent EPR intensities I_{EPR}, which are proportional to the magnetic susceptibilities ($\chi \propto I_{EPR}$) were extracted from the temperature-dependent X-band spectra (Figure 7 in Appendix C) as derived by full double integration of the corresponding spectra. The insets of Figure 2 show their corresponding inverse intensity I_{EPR}^{-1} as a function of temperature and fitted using C-W law, eqn. 4. The EPR intensities provide θ_p = -70 K and -85 K for MIL-101(Cr) and MIL-100(Al$_{0.8}$Cr$_{0.2}$), respectively, from the C-W fit which is in reasonable agreement with the θ_p values found from the magnetization susceptibility data and once again suggest the existence of antiferromagnetic interactions in both materials.
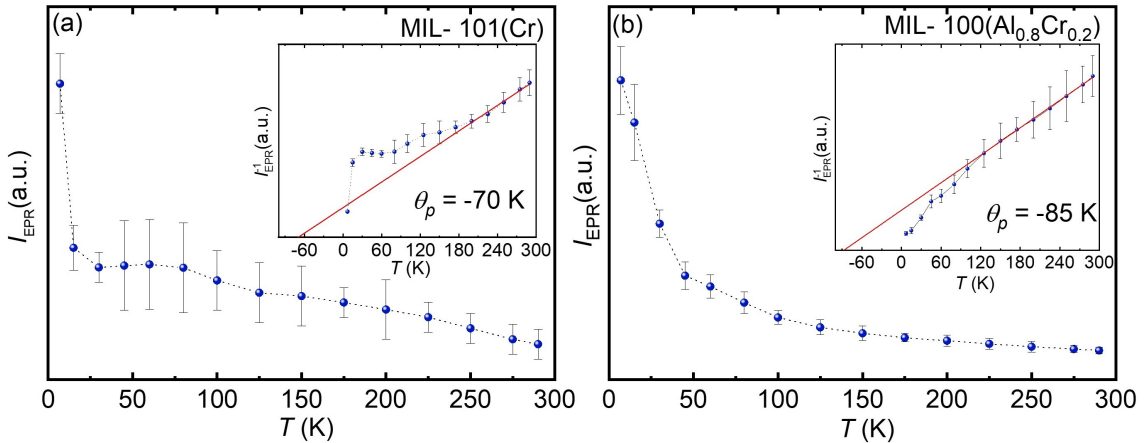
Figure 2: EPR Intensities (I_{EPR}) belong to Cr(III) spectra of (a) MIL-101(Cr), and (b) MIL-100(Al$_{0.8}$Cr$_{0.2}$) extracted from temperature-dependent X-band EPR data. (Inset: Corresponding C-W fit of I_{EPR}^{-1} as a function of temperature.)

Figure 3 shows the multi-frequency EPR spectra of MIL-101(Cr) and MIL-100(Al$_{0.8}$Cr$_{0.2}$) MOFs at room and low temperatures. A full temperature dependence EPR X-band spectra for both samples are illustrated in Figure. 7 (Appendix C).

Unlike MIL-100(Al$_{0.8}$Cr$_{0.2}$), a significant shift in the *g*-value of the major signal A with g_A = 1.979 at 290 K towards smaller *g*-values of g_E = 1.945 (signal E at 20 K) and g_B = 1.779 (signal B at 7 K) is observed for MIL-101(Cr) (Figure 3). The change in *g* as a function of temperature for MIL-101(Cr) is given in Figure 8a (Appendix C) together with that of MIL- 100(Al$_{0.8}$Cr$_{0.2}$) for comparison. We have to note that typical *g*-values for both isolated and coupled Cr(III) ions are in the range of *g* = 1.97 – 1.98 [22]. Honda *et al.* [12] discussed a comparable anomalous *g*-shift for Cr(III)$_3$ trimers in Cr-acetate and Cr-propionate. Such signals with characteristic *g*-shifts at low temperatures have also been reported for AFM coupled Cr(III)$_3$ trimers in other
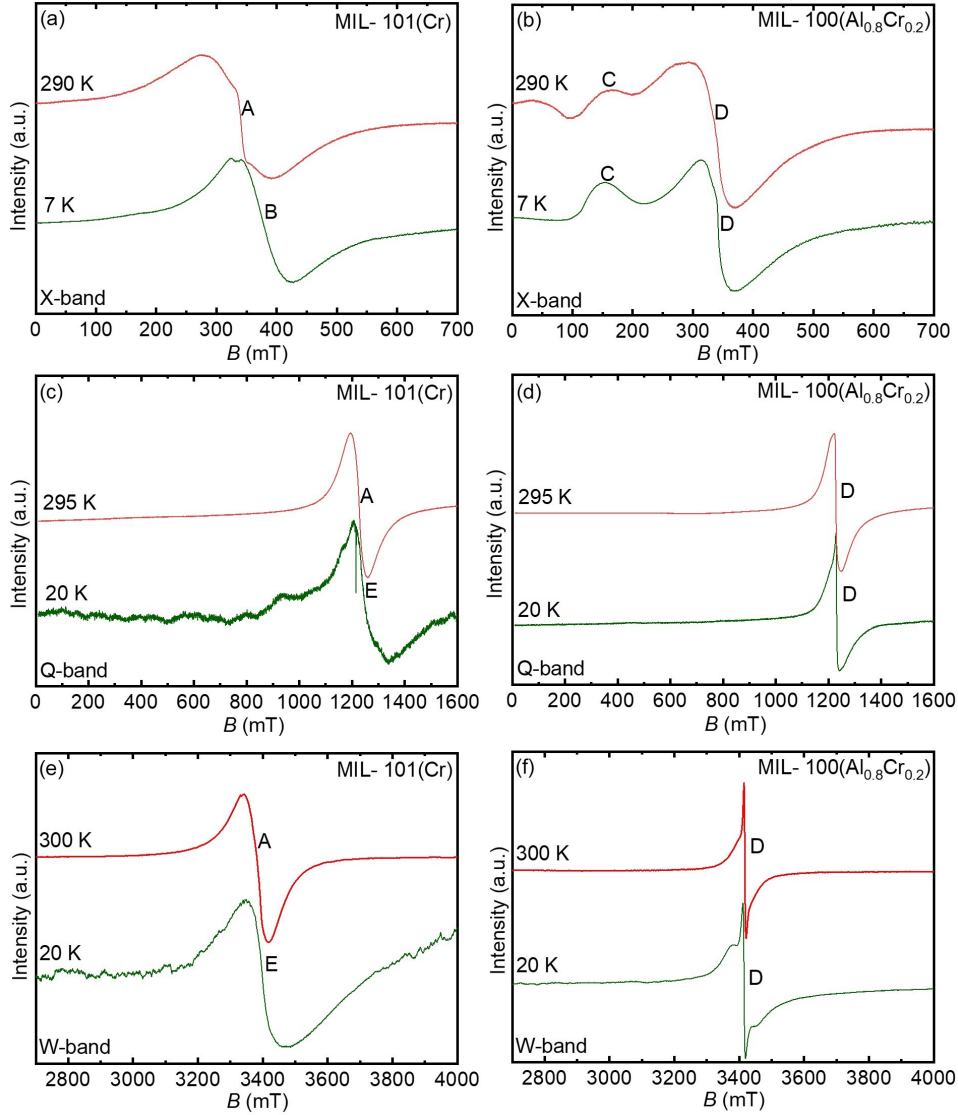
Figure 3: (a & b) X-band, (c & d) Q-band and (e & f) W-band EPR spectra of MIL-101(Cr) and MIL-100($Al_{0.8}Cr_{0.2}$) MOFs, respectively. (*g*-values of the corresponding signals: $g_A = 1.979$, $g_B = 1.779$, $g_C = $ 5.5 - 4.0 , $g_D = 1.973$ and $g_E = 1.945$)

matrices [13,23] and were assigned to their ground state with the total spin $S_T = 1/2$ [12,13,23].

The effective *g*-value of this doublet ground state is approximated by [12,13,23]

$$g_{eff} \approx g_A \sqrt{1 - \frac{48d^2}{(16J_1^2 + 48d^2) - (\mu_B B g_A)^2}} \tag{8}$$

Here, $d = D_{12,z} + D_{23,z} + D_{13,z}$ is the asymmetric exchange parameter of the trimer according to the D-M interaction and $\sqrt{16J_1^2 + 48d^2}$ corresponds to the splitting between the $S_T = \frac{1}{2}$ ground state and the first excited state of the trimer having likewise $S_T = \frac{1}{2}$. As J_1 is not known for MIL-101(Cr), we cannot derive the value of d from our experimental results. However, the observed characteristic *g*-shift of the doublet ground state at $T < 30$ K can be considered as a signature for AFM coupled $Cr(III)_3$ trimers. On the other hand, the almost isotropic EPR signal at higher temperatures is less indicative of AFM coupling as all total spin

levels $S_T = 1/2, 3/2, \ldots, 9/2$ will be more populated depending on the temperature and degeneracy.

The X-band EPR spectrum of MIL- 100($Al_{0.8}Cr_{0.2}$) (Figure 3a) appears to be more complex as at least two signals C and D having $g_C = 4.0 - 5.5$ and , $g_D = 1.973$, respectively can be discerned in the whole temperature range (Figure 7b in Appendix C). However, besides some decrease in the line-widths towards lower temperatures, (Figure 8b in Appendix C) the spectra reveal no characteristic temperature-dependence of the g values of signals C and, in particular of signal D even at $T = 7$ K (Figure 8a in Appendix C). In addition, the line-width of signal D is significantly smaller than that of signal A in MIL-101(Cr) (Figure 8b). Therefore, we can exclude the formation of AFM coupled Cr(III)$_3$ trimers for MIL- 100($Al_{0.8}Cr_{0.2}$).

EPR spectra comparable to those of MIL- 100($Al_{0.8}Cr_{0.2}$) have been reported for Cr(III) doped phosphate glasses [22] and microporous materials such as silica and various zeolite type frameworks [24], and the signals C and D have been identified there. Signal C is assigned to isolated high-spin Cr(III) ions with $S = 3/2$ in a highly distorted octahedral oxygen ion coordination. This gives rise to large variations in the E_{ZFS}/D_{ZFS} ratios ($0 < E_{ZFS}/D_{ZFS} < 1/3$) leading for $D_{ZFS} > \mu_B B g_C$ to g-values between $4.0 - 5.5$. This condition is often met for X-band EPR spectroscopy but may not hold any longer at higher fields [24]. Therefore only a single line at $g = 1.97 - 1.98$ is observed in the Q- and W-band spectra in Figures 3d and 3f. The presence of isolated Cr(III) species is supported by the most likely paramagnetic response in the low-temperature magnetization date of MIL- 100($Al_{0.8}Cr_{0.2}$) (Figure 1b). According to previous assignments, signal D is caused either by AFM exchanged coupled Cr(III)$_2$ pairs [22] or Cr(III)$_x$O$_y$ clusters [24]. Therefore, it seems to be justified to assign signals C and D to Al(III)$_2$Cr(III)$_1$ and Al(III)$_1$Cr(III)$_2$ units in MIL- 100($Al_{0.8}Cr_{0.2}$). Similar mixed metal ion trimers have been identified in MOF MIL-100($Al_{3-x}Fe_x$) [25].

4 Conclusion

Magnetization and EPR measurements confirm the formation of AFM coupled Cr(III)$_3$ trimers in the MOF MIL-101(Cr), having an exchange coupling constant J_0 = -11.4 cm^{-1}. The trimers in the supertetrahedral building units of the MIL-101(Cr) framework are weakly coupled, as indicated by the determined small inter-trimer exchange interaction. The doublet total spin ground state of the Cr(III)$_3$ trimers reveals D-M interaction leading to a characteristic shift of its g-value shift at low temperatures. Although the magnetically diluted MOF MIL- 100($Al_{0.8}Cr_{0.2}$) displays AFM properties likewise the temperature-independent g-values of the Cr(III) EPR signals indicate that Cr(III)$_3$ trimers are not formed, and the Cr(III) ions are dispersed over the framework. We suggest that Cr(III) is incorporated as paramagnetic Al(III)$_2$Cr(III)$_1$ and AFM coupled Al(III)$_1$Cr(III)$_2$ trimeric metal ion units into the MIL-100 framework though we cannot completely exclude the formation of minor isolated and clustered extra-framework chromium species.

Acknowledgements

The authors, K. Thangavel., D. M. Murphy, and A. Pöppl. from Leipzig and Cardiff universities, gratefully acknowledge funding from the European Union's Horizon 2020 research and innovation programme under the Marie Skłodowska Curie Actions- PARACAT(paramagnetic species in catalysis research) grant agreement No 813209.

Author contributions K.T carried out the X- and Q-band EPR studies. W-band measurements were performed by A.F and K.T. SQUID measurements were done by M. Z. Team TUD offered MOFs with preliminary characterizations. K.T and A.P wrote the manuscript, and all authors have contributed and approved the final manuscript.

Funding information: Visit PARACAT to know the technical information about the project and PARACAT-CORDIS for the official information.

Appendix

A Structure of trimer complex in MIL-101 and MIL-100 MOFs
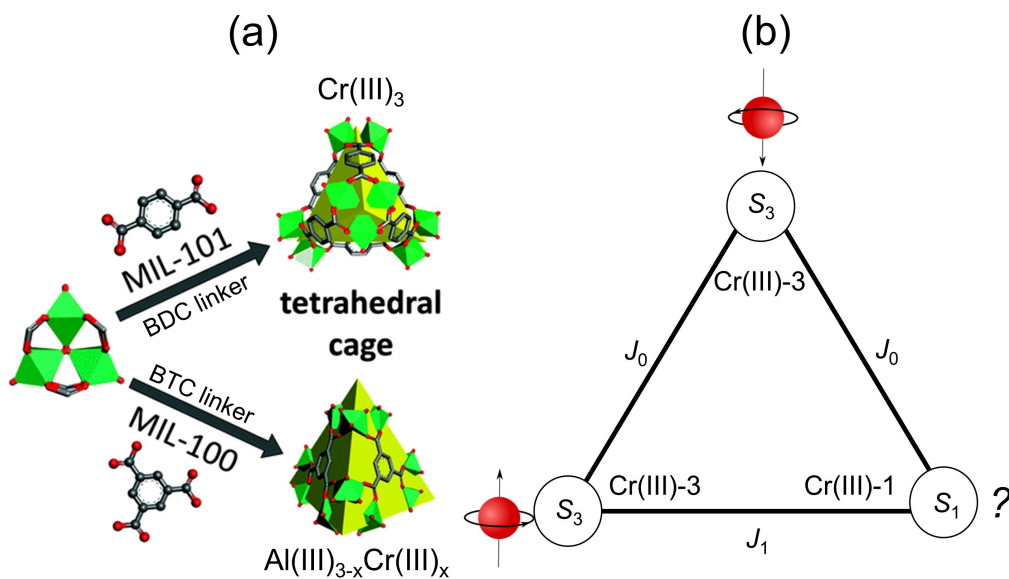
Figure 4: (a) Cr(III)/Al(III) ions are in the octahedral trimer units and four trimers, forming a supertetrahedra (A small portion of the image adapted from B. Van *et al* [8]) showing MIL-101(Cr) and MIL-100($Al_{0.8}Cr_{0.2}$) (b) Scheme of the equilaterial triangle contains three $S = 3/2$ Cr(III) spins shows the situation of spin 'frustration' (J_0 and J_1 are the exchange coupling parameters).

Four trimers together make super-tetrahedra cage through BTC linker (MIL-100) and BDC linker (MIL-101).

Table 1: Paramagnetic Curie temperature (θ_p), effective magnetic moment (μ_{eff}) and Curie constant values of MIL-100(Cr) and MIL-101(Al$_{0.8}$Cr$_{0.2}$) from SQUID and EPR measurements.

MOFs	Measurement	θ_p (K)	μ_{eff} (μ_B/f.u.)	C
MIL-101(Cr)	SQUID	-82	5.43	3.69
	EPR	-70	-	-
MIL-100 (Al$_{0.8}$Cr$_{0.2}$)	SQUID	-87	3.14	1.23
	EPR	-85	-	-

B   Supplementary Magnetization results
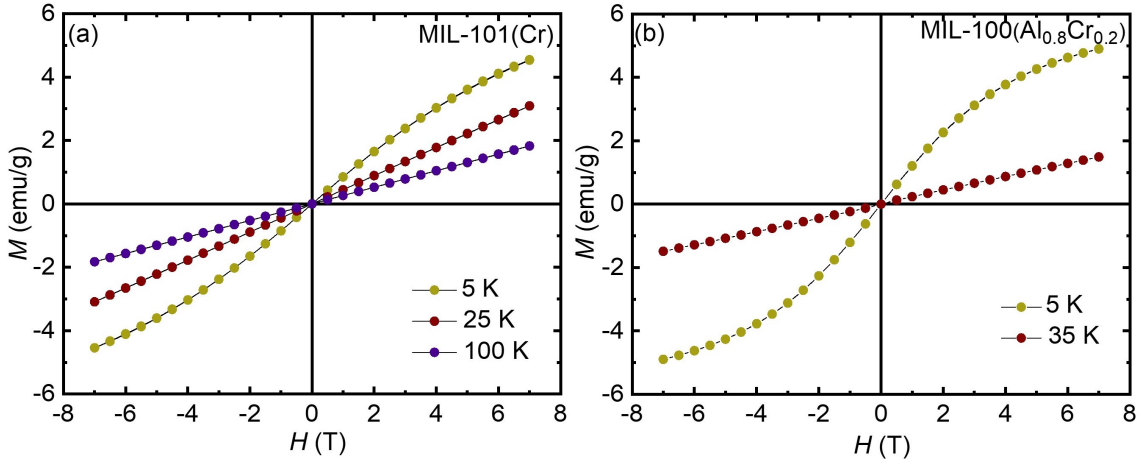
Figure 5: *M-H* curves recorded at 5 K, 25 K and 100 K for (a) MIL-101(Cr) and, 5 K and 35 K for (b) MIL-100(Al$_{0.8}$Cr$_{0.2}$).

The field-dependent magnetization measured at $T = 5$ K, 25 K and 100 K for MIL-101(Cr) and, at $T = 5$ K and 35 K for MIL-100(Al$_{0.8}$Cr$_{0.2}$) show a linear increase of magnetization with field up to 7 T . No magnetic hysteresis behavior was observed.
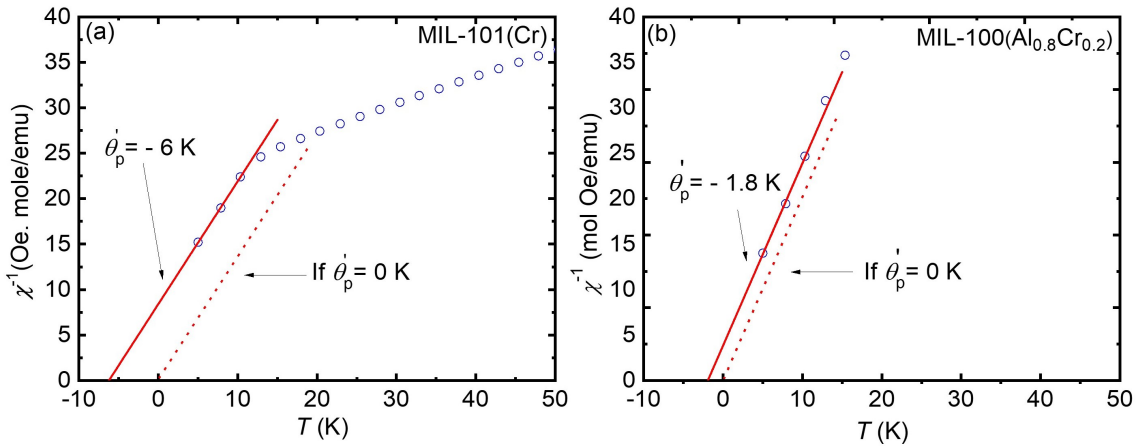
Figure 6: C-W fit on the temperature-dependent reciprocal of the magnetic susceptibility of (a) MIL-101(Cr) and (b) MIL-100(Al$_{0.8}$Cr$_{0.2}$) below $T < 15$ K.

Table 2: Comparison of magnetization values for the MIL-101(Cr) and MIL-100($Al_{0.8}Cr_{0.2}$) MOFs found from *M-T* and *M-H* curves at the 5 K, 25 K, 35 K and 100 K temperatures

MOFs	H (T)	M (emu/g)				
		at 5 K	at 25 K	at 35 K	at 100 K	300 K
MIL-101(Cr)	(*M-H*)7 T	4.54	3.12	-	1.81	-
	(*M-H*)0.5 T	0.44	0.23	-	0.12	-
	(*M-T*)0.5 T	0.44	0.23	0.21	0.13	0.06
MIL-100	(*M-H*)7 T	4.95	-	1.47	-	-
($Al_{0.8}Cr_{0.2}$)	(*M-H*)0.5 T	0.59	-	0.12	-	-
	(*M-T*) 0.5 T	0.59	0.16	0.12	0.06	0.00

C   Supplementary EPR results

Figure 7 illustrates a series of temperature-dependent X-band EPR data of MIL-100(Cr) and MIL-100($Al_{0.8}Cr_{0.2}$) materials.
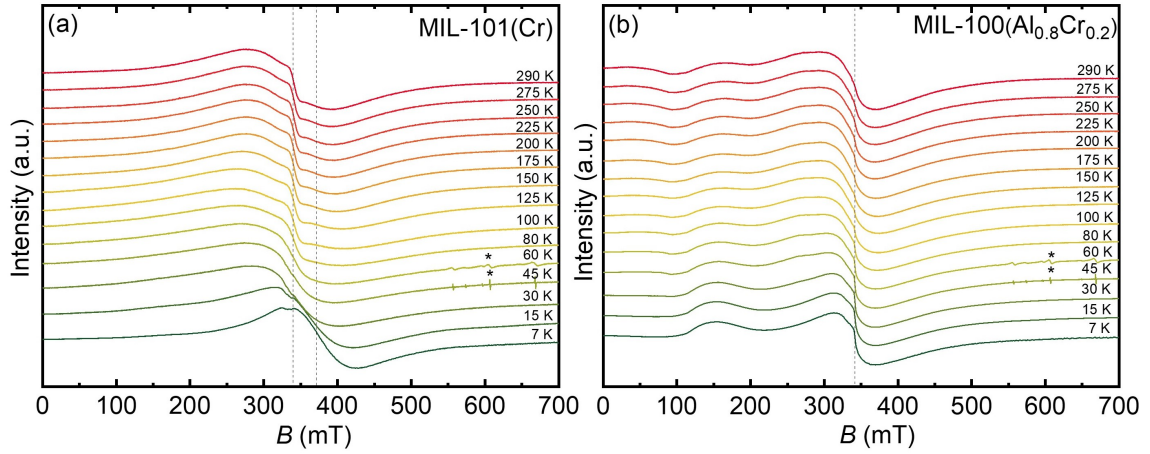
Figure 7: Temperature-dependent X -band EPR data of (a) MIL-101(Cr) and (b) MIL-100($Al_{0.8}Cr_{0.2}$) at temperature ranging from $T = 7$ K to $T = 290$ K(*-corresponds to the gaseous oxygen in the cryostat).
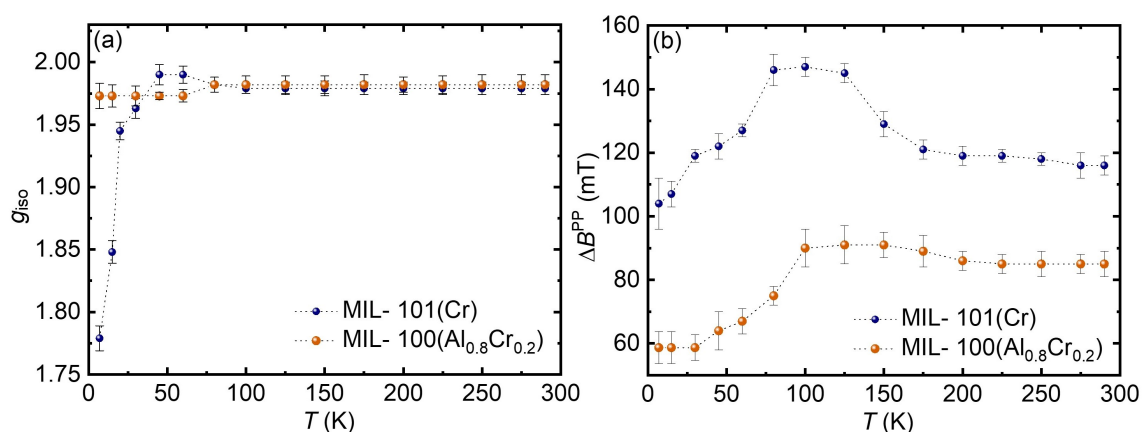
Figure 8: Temperature-dependent (a) g_{iso} trend, and (b) peak to peak width (ΔB_{pp}) of MIL-101(Cr) and MIL-100(Al$_{0.8}$Cr$_{0.2}$) extracted form the X-band temperature-dependent spectra.

References

[1] M. Bracci, P. C. Bruzzese, A. Famulari, D. Fioco, A. Guidetti, Y.-K. Liao, L. Podvorica, S. F. Rezayi, I. Serra, K. Thangavel and D. M. Murphy, *Paramagnetic species in catalysis research: a unified approach towards (the role of epr in) heterogeneous, homogeneous and enzyme catalysis*, Electron Paramag. Reson. **27**, 1 (2021), doi:10.1039/9781839162534-00001.

[2] J. Bitzer, S. Otterbach, K. Thangavel, A. Kultaeva, R. Schmid, A. Pöppl and W. Kleist, *Experimental evidence for the incorporation of two metals at equivalent lattice positions in mixed-metal metal–organic frameworks*, Chem. Eur. J. **26**(25), 5667 (2020), doi:10.1002/chem.201905596.

[3] A. U. Czaja, N. Trukhan and U. Müller, *Industrial applications of metal–organic frameworks*, Chem. Soc. Rev. **38**(5), 1284 (2009), doi:10.1039/b804680h.

[4] J. Casaban, Y. Zhang, R. Pacheco, C. Coney, C. Holmes, E. Sutherland, C. Hamill, J. Breen, S. L. James, D. Tufano *et al.*, *Towards mofs' mass market adoption: Mof technologies' efficient and versatile one-step extrusion of shaped mofs directly from raw materials*, Faraday Discuss. **231**, 312 (2021), doi:10.1039/d1fd00025j.

[5] P. Falcaro, R. Ricco, C. M. Doherty, K. Liang, A. J. Hill and M. J. Styles, *Mof positioning technology and device fabrication*, Chem. Soc. Rev. **43**(16), 5513 (2014), doi:10.1039/C4CS00089G.

[6] G. M. Espallargas and E. Coronado, *Magnetic functionalities in mofs: from the framework to the pore*, Chem. Soc. Rev. **47**(2), 533 (2018), doi:10.1039/C7CS00653E.

[7] G. Zhong, D. Liu and J. Zhang, *Applications of porous metal–organic framework mil-100 (m)(m= cr, fe, sc, al, v)*, Cryst. Growth Des. **18**(12), 7730 (2018), doi:10.1021/acs.cgd.8b01353.

[8] B. Van de Voorde, B. Bueken, J. Denayer and D. De Vos, *Adsorptive separation on metal–organic frameworks in the liquid phase*, Chem.Soc. Rev. **43**(16), 5766 (2014), doi:10.1039/C4CS00006D.

[9] M. D'Amore, B. Civalleri, I. J. Bush, E. Albanese and M. Ferrabone, *Elucidating the interaction of co2 in the giant metal–organic framework mil-100 through large-scale periodic ab initio modeling*, J. Phys. Chem. C **123**(47), 28677 (2019), doi:10.1021/acs.jpcc.9b06533.

[10] S. Ferrer, F. Lloret, E. Pardo, J. M. Clemente-Juan, M. Liu-Gonzalez and S. García-Granda, *Antisymmetric exchange in triangular tricopper (ii) complexes: correlation among structural, magnetic, and electron paramagnetic resonance parameters*, Inorg. Chem. **51**(2), 985 (2012), doi:10.1021/ic2020034.

[11] B. Tsukerblat, B. Y. Kuyavskaya, M. Belinskii, A. Ablov, V. Novotortsev and V. Kalinnikov, *Antisymmetric exchange in the trinuclear clusters of copper (ii)*, Theor. Chim. Acta. **38**(2), 131 (1975), doi:10.1007/BF00581470.

[12] M. Honda, M. Morita and M. Date, *Electron spin resonance in cr-trimer complexes*, J. Phys. Soc. Jpn. **61**(10), 3773 (1992), doi:10.1143/JPSJ.61.3773.

[13] A. Vlachos, V. Psycharis, C. P. Raptopoulou, N. Lalioti, Y. Sanakis, G. Diamantopoulos, M. Fardis, M. Karayanni, G. Papavassiliou and A. Terzis, *A nearly symmetric trinuclear chromium (iii) oxo carboxylate assembly: preparation, molecular and crystal structure, and magnetic properties of [cr3o (o2cph) 6 (meoh) 3](no3)· 2meoh*, Inorganica Chim. Acta. **357**(11), 3162 (2004), doi:10.1016/j.ica.2004.04.005.

[14] A. Figuerola, V. Tangoulis, J. Ribas, H. Hartl, I. Brüdgam, M. Maestro and C. Diaz, *Synthesis, crystal structure, and magnetic studies of oxo-centered trinuclear chromium (iii) complexes:[cr3 (μ3-o)(μ2-phcoo) 6 (h2o) 3] no3 4h2o 2ch3oh, a case of spin-frustrated system, and [cr3 (μ3-o)-(μ2-phcoo) 2 (μ2-och2ch3) 2 (bpy) 2 (ncs) 3], a new type of [cr3o] core*, Inorg. Chem. **46**(26), 11017 (2007), doi:10.1021/ic700606e.

[15] M. Mendt, P. Vervoorts, A. Schneemann, R. A. Fischer and A. Poppl, *Probing local structural changes at cu2+ in a flexible mixed-metal metal-organic framework by in situ electron paramagnetic resonance during co2 ad-and desorption*, J. Phys. Chem. C **123**(5), 2940 (2019), doi:10.1021/acs.jpcc.8b10661.

[16] M. Mendt, B. Barth, M. Hartmann and A. Pöppl, *Low-temperature binding of no adsorbed on mil-100 (al)—a case study for the application of high resolution pulsed epr methods and dft calculations*, J. Chem. Phys. **147**(22), 224701 (2017), doi:10.1063/1.4995551.

[17] D. M. Polyukhov, S. Krause, V. Bon, A. S. Poryvaev, S. Kaskel and M. V. Fedin, *Structural transitions of the metal–organic framework dut-49 (cu) upon physi-and chemisorption studied by in situ electron paramagnetic resonance spectroscopy*, J. Phys. Chem. Lett. **11**(15), 5856 (2020), doi:10.1021/acs.jpclett.0c01705.

[18] T. Wittmann, A. Mondal, C. B. Tschense, J. J. Wittmann, O. Klimm, R. Siegel, B. Corzilius, B. Weber, M. Kaupp and J. Senker, *Probing interactions of n-donor molecules with open metal sites within paramagnetic cr-mil-101: a solid-state nmr spectroscopic and density functional theory study*, J. Am. Chem. Soc. **140**(6), 2135 (2018), doi:10.1021/jacs.7b10148.

[19] A. Pöppl, S. Kunz, D. Himsl and M. Hartmann, *Cw and pulsed esr spectroscopy of cupric ions in the metal- organic framework compound cu3 (btc) 2*, J. Phys. Chem. C **112**(7), 2678 (2008), doi:10.1021/jp7100094.

[20] A. Kultaeva, T. Biktagirov, P. Neugebauer, H. Bamberger, J. Bergmann, J. van Slageren, H. Krautscheid and A. Poppl, *Multifrequency epr, squid, and dft study of cupric ions and their magnetic coupling in the metal–organic framework compound 3 [cu (prz–trz–ia)]*, J. Phys. Chem. C **122**(46), 26642 (2018), doi:10.1021/acs.jpcc.8b08327.

[21] S. J. Miyake, *Spin-wave results for the staggered magnetization of triangular heisenberg antiferromagnet*, J. Phys. Soc. Jpn. **61**(3), 983 (1992), doi:10.1143/JPSJ.61.983.

[22] R. Landry, J. Fournier and C. Young, *Electron spin resonance and optical absorption studies of cr3+ in a phosphate glass*, J. Chem. Phys. **46**(4), 1285 (1967), doi:10.1063/1.1840846.

[23] V. Psycharis, C. P. Raptopoulou, A. K. Boudalis, Y. Sanakis, M. Fardis, G. Diamantopoulos and G. Papavassiliou, *Syntheses, structural, and physical studies of basic CrIII and FeIII benzilates and benzoates: Evidence of antisymmetric exchange and distributions of isotropic and antisymmetric exchange parameters*, Eur. J. Inorg. Chem. **2006**(18), 3710, doi:10.1002/ejic.200600306.

[24] B. M. Weckhuysen, R. A. Schoonheydt, F. E. Mabbs and D. Collison, *Electron paramagnetic resonance of heterogeneous chromium catalysts*, J. chem. Soc., Faraday Trans. **92**(13), 2431 (1996), doi:10.1039/FT9969202431.

[25] G. Mali, M. Mazaj, I. Arcon, D. Hanzel, D. Arcon and Z. k. Jaglicic, *Unraveling the arrangement of al and fe within the framework explains the magnetism of mixed-metal mil-100 (al, fe)*, J. Phys. Chem. Lett. **10**(7), 1464 (2019), doi:10.1021/acs.jpclett.9b00341.